





Strong coupling between excitons and quasibound states in the continuum in bulk transition metal dichalcogenides

Meibao Qin ¹, Junyi Duan,^{2,3,*} Shuyuan Xiao ^{2,3}, Wenxing Liu ¹, Tianbao Yu ^{1,†}, Tongbiao Wang,¹ and Qinghua Liao¹

¹*Department of Physics, Nanchang University, Nanchang 330031, People's Republic of China*

²*Institute for Advanced Study, Nanchang University, Nanchang 330031, People's Republic of China*

³*Jiangxi Key Laboratory for Microscale Interdisciplinary Study, Nanchang University, Nanchang 330031, People's Republic of China*



(Received 1 September 2022; revised 8 November 2022; accepted 9 January 2023; published 17 January 2023)

We investigate the strong coupling between excitons and quasibound states in the continuum (BICs) resonance in a bulk WS_2 metasurface. Here, we employ bulk WS_2 to construct an ultrathin nanodisk metasurface, supporting the symmetry-protected magnetic dipole quasi-BIC resonance, which can self-hybridize with the excitons and lead to a strong light-matter interaction enhancement within the structure without the necessity for an external cavity. This strong coupling can be characterized by the considerable Rabi splitting of 159 meV and the clearly anticrossing behavior appearing in the absorption spectrum. Furthermore, we analyze such light-matter coupling by constructing a Hamiltonian model including the surplus excitons and tune the interaction from weak- to strong-coupling regimes via the tunability radiation loss of the quasi-BIC resonance. Our results have great potential for manipulating the exciton-polaritons at room temperature and provide a promising prospect for photonic devices that exploit strong coupling in applications.

DOI: [10.1103/PhysRevB.107.045417](https://doi.org/10.1103/PhysRevB.107.045417)

I. INTRODUCTION

Strong coupling, allowing energy to exist between light and matter in a coherent and reversible manner, has emerged as a growing range of applications such as Bose-Einstein condensation, superfluidity, spin switch, and lasing [1–5]. It has been demonstrated that strong coupling can be easily achieved at room temperature by integrating excitons in monolayer transition metal dichalcogenides (TMDCs) into plasmonic/dielectric cavities [6–13]. However, plasmonic materials suffer from low damage thresholds, making them bottlenecked in further practical applications [14–16]. High-refractive dielectric resonators support the Mie resonance without ohmic loss but confine the electric field to the internal part of the structure, resulting in a small Rabi splitting [17–19]. Quasibound states in the continuum (BICs) possess the characteristics of high Q and the ability to exchange energy with other modes, which enables BICs suitable for various applications in enhancing the interaction between light and matter [20–23], which show a prospect for overcoming this barrier. Nevertheless, the spatial overlap between excitons and quasi-BICs remains not enough to realize a large Rabi splitting [24–31].

Bulk TMDCs are featured by the strong exciton absorption peak and high refractive index, making the spatial overlap between excitons and the optical resonance mode in the same structure possible, which provide promising candidates for boosting strong coupling [32,33]. According to the literature, very large values of Rabi splitting have been observed

in some bulk TMDC cavities, including Fabry-Perot microcavities, anapole states in a nanodisk, and quasi-BICs in a one-dimensional grating [32,34,35]. However, there are few reports on the strong exciton–BIC coupling in a bulk TMDC metasurface, and particularly the surplus excitons in the coupling region and their line-width influence on the light-matter absorption spectrum need to be explored.

In this paper, we study the strong exciton–BIC interaction in a bulk TMDC metasurface. We design a self-hybridized exciton-polariton nanodisk metasurface by employing bulk WS_2 , in which the spatial overlap between the symmetry-protected magnetic dipole (MD) quasi-BIC resonance and the exciton mode can be realized, resulting in a large Rabi splitting of 159 meV. This strong coupling could be further demonstrated by the anticrossing behavior in the absorption spectrum. Furthermore, we construct a Hamiltonian model involving the surplus excitons to interpret the coupling condition, which makes it possible to tune the absorption spectrum by adjusting the asymmetry parameter.

II. GEOMETRIC STRUCTURE AND NUMERICAL MODEL

The proposed model is schematically shown in Fig. 1(a). A nanodisk metasurface made out of bulk WS_2 is deposited onto a SiO_2 substrate, illuminated by a normally incident plane wave. The periodicity of each unit cell is $P = 370$ nm. Every disk has a radius $R = 110$ nm and a height $H = 35$ nm. A hole with variable radius r at a fixed distance $D = R/2$ away from the center of the disk and the asymmetry parameter $\alpha = \frac{\pi r^2}{\pi R^2}$ is characterized by the ratio of the hole area to the nanodisk area. This in-plane perturbation of the structure will open a radiation channel, enabling an energy change with the external mode by transforming the ideal BIC into a quasi-BIC.

*jyduan@email.ncu.edu.cn

†yutianbao@ncu.edu.cn

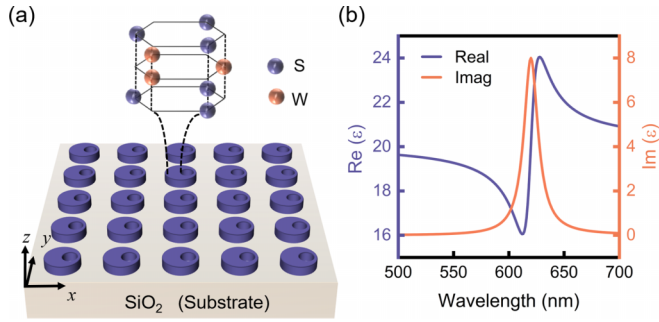


FIG. 1. (a) Sketch of the system: Nanodisk metasurfaces of bulk WS_2 are illuminated by a normally incident plane wave. (b) The dielectric functions of bulk WS_2 ; blue and red lines represent real and imaginary parts, respectively.

The full-wave electromagnetic response simulation is carried out using the COMSOL MULTIPHYSICS based on the finite element method. In the simulation domain, the y -polarized plane wave is normally incident, and the perfectly matched layers are utilized to absorb the outgoing radiated wave in the z direction, with periodic boundary conditions in the x and y directions due to the periodicity of nanodisk metasurfaces. For the material modeling, we choose bulk WS_2 as the constituent due to its high permittivity, as depicted in Fig. 1(b). The artificial permittivity approximation of bulk WS_2 in Fig. 1(b) can be described by [32,34,36]

$$\varepsilon_{\text{art}} = \varepsilon_b + \frac{f_0 E_{\text{ex}}^2}{E_{\text{ex}}^2 - E^2 - i\Gamma_{\text{ex}} E}, \quad (1)$$

where $\varepsilon_b = 20$ represents the background permittivity, $f_0 = 0.2$ is the oscillator strength, $E_{\text{ex}} = 2$ eV and $\Gamma_{\text{ex}} = 50$ meV are transition energy and full linewidth of the exciton, respectively. For background index-only material, f_0 is set to be 0. For an exciton-only material, ε_b is set to be 1, while the other parameters remain unchanged.

III. RESULTS AND DISCUSSION

To confirm the existence of the BIC in our proposed bulk WS_2 nanodisk metasurface, we setting the oscillator strength $f_0 = 0$ and then perform an eigenmode analysis without the substrate. In Fig. 2(a), a band diagram along $X-\Gamma-X'$ for transverse electric (TE)-like mode ~ 665 nm in the first Brillouin zone is shown. In the following analysis of the eigenmode at the Γ point in Fig. 2(b), we can see that the Q factor is $> 10^{10}$. According to the symmetry of the modes referring to the C_{2v} group, when the normally incident plane wave is TE polarized, electric fields show an odd symmetry with respect to the z axis. Therefore, H_z is an even mode decoupling from the radiation mode because the plane wave is an odd mode under a normal incident around the z axis, which is called the symmetric-protected BIC. Furthermore, we show the simulated transmission spectra of the nanodisk metasurface as a function of the asymmetry parameters in the following two case. For the freestanding nanodisk metasurface, Fig. 2(c) exhibits an ideal BIC with vanished linewidth ~ 665 nm. For the realistic case where the substrate is considered in Fig. 2(d), we find the ideal BIC appearing at 680 nm slightly redshifted

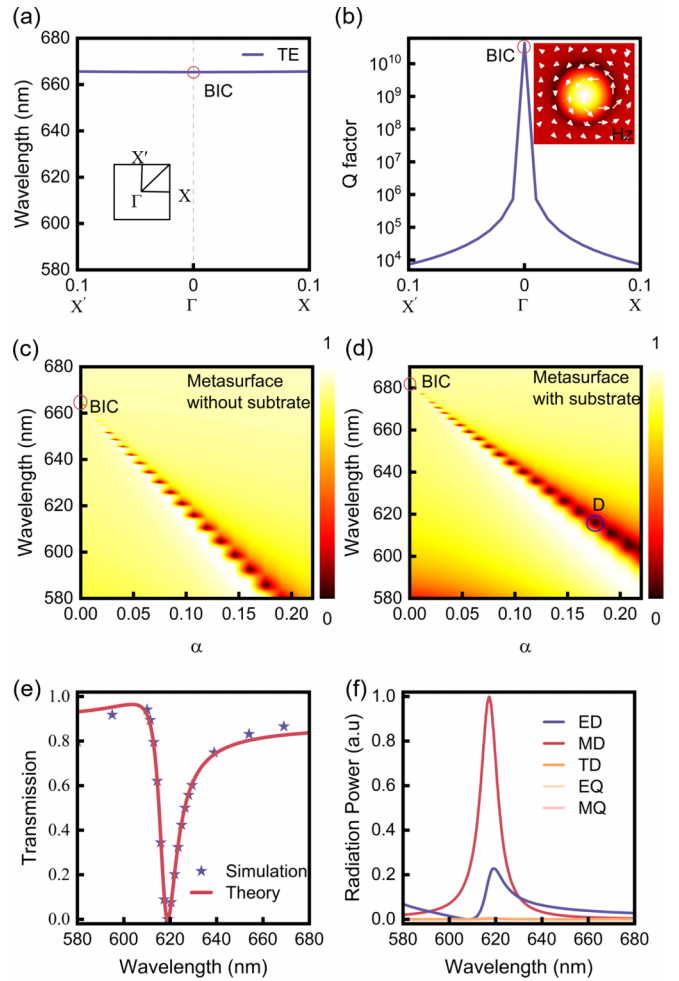


FIG. 2. (a) Band diagrams of the bulk WS_2 nanodisk metasurfaces without substrate. Here, $P = 370$ nm, $R = 110$ nm, and $H = 35$ nm. The symmetry-protected bound state in the continuum (BIC) is marked with a red circle. (b) The corresponding Q factors for the transverse electric (TE)-like ~ 665 nm, and the inset shows the corresponding magnetic distribution of H_z at the point ~ 665 nm overlaid with the in-plane electric field direction vector E_{xy} . (c) The transmission spectra of bulk WS_2 nanodisk metasurfaces as a function of the asymmetric parameter without substrate, where an ideal BIC is marked by a red circle. (d) The transmission spectra of bulk WS_2 nanodisk metasurfaces as a function of the asymmetric parameter with SiO_2 substrate, where an ideal BIC is marked by a red circle and the D point around the exciton position of 620 nm. (e) The simulated and theoretical transmission spectra of the D point. (f) The scattered power of the multipole moments under the Cartesian coordinates.

compared with the freestanding case. To further show that the substrate only shifts the resonance of the quasi-BIC but not its modal properties, we perform a transmission spectrum of $\alpha = 0.17$ [the D point of Fig. 2(d)], as displayed in Fig. 2(e). The sharp resonance can be well fitted by the Fano formula, which shows that the ideal BIC is transformed into a quasi-BIC by breaking the in-plane symmetry of the unit cell with the exchange of energy. To identify the electromagnetic mode origin of the observed quasi-BIC resonance, we calculate the multipolar decomposition of the optical response under the

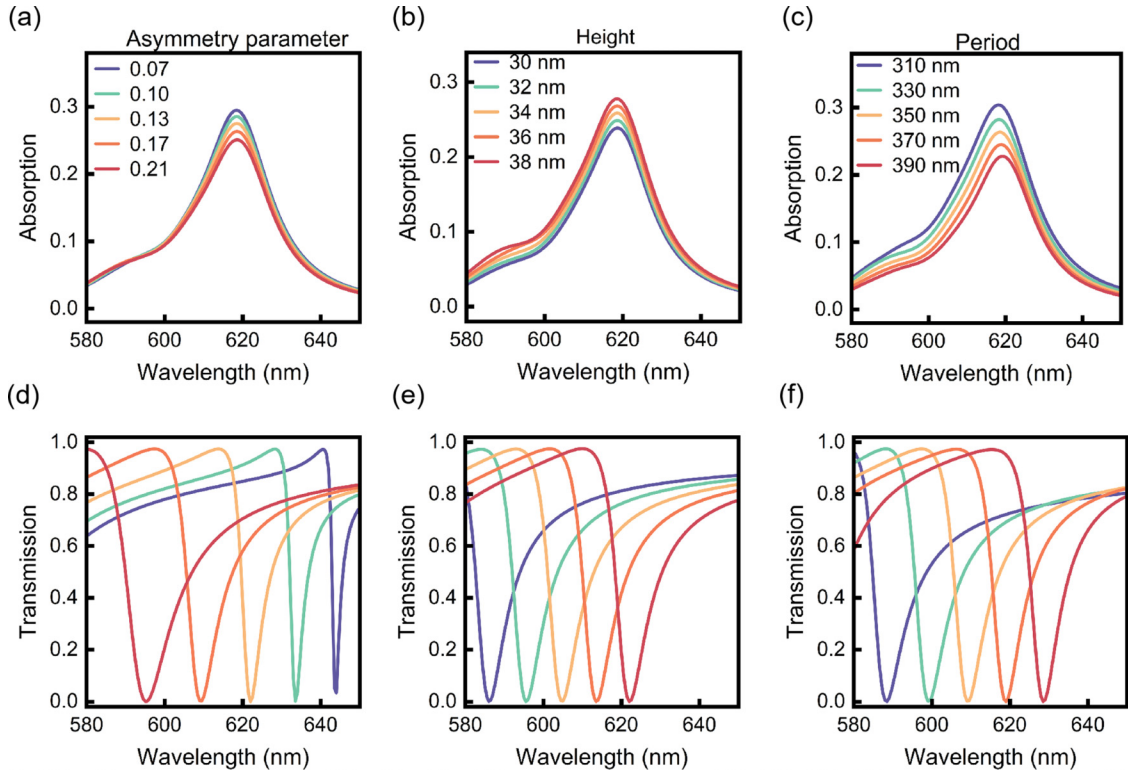


FIG. 3. The effect of structural parameters on the exciton mode ($\varepsilon_b = 1$) and the quasibound state in the continuum (BIC) mode ($f_0 = 0$). (a) and (d) show the absorption spectrum of the exciton mode and the transmission spectrum of the quasi-BIC mode for different asymmetry parameters, where $P = 370$ nm and $H = 35$ nm. (b) and (e) show the absorption spectra of the exciton mode and the transmission spectra of the quasi-BIC mode for different heights, where $P = 370$ nm and $\alpha = 0.17$. (c) and (f) show the absorption spectra of the exciton mode and the transmission spectra of the quasi-BIC mode for different periods, where $\alpha = 0.17$ and $H = 35$ nm.

Cartesian coordinates in Fig. 2(f), and it is clear that the dominant contribution at resonance is provided by the MD, which is consistent with the analysis of the previously mentioned H_z results.

To facilitate the design of the self-hybridized exciton-polaritons in the bulk WS_2 nanodisk metasurface, we study the optical response of the exciton mode ($\varepsilon_b = 1$) and the quasi-BIC mode ($f_0 = 0$) with different structure parameters. In Figs. 3(a)–3(c), we plot the absorption spectrum of the exciton mode for different structure parameters. From these results, it can be found that the absorption of the exciton mode will increase with the height, which shows the opposite trend with the increase of the asymmetry parameter and period due to the decrease of the filling ratio. It is worth noticing that the position of the exciton mode still locates ~ 620 nm. In Figs. 3(d) and 3(f), the linewidth of the MD quasi-BIC mode is sensitive to the increase of the asymmetry parameter. The position of the MD quasi-BIC resonance shows a clear redshift in the transmission spectra with the increase of the period and height, which shows the opposite trend with the increase of the asymmetry parameter. These make it possible to manipulate the linewidth by adjusting the asymmetry parameter and the resonance position through changing the period. The implementation of strong coupling in a bulk WS_2 metasurface needs the linewidth and the resonance position of the MD quasi-BIC to be close to that of the exciton mode. The linewidth coincidence can be achieved by adjusting the

asymmetry parameter, and the resonance position coincidence can be obtained by adjusting the period. The thicker the nanodisk is, the higher the absorption peak of excitons can be observed in Fig. 3(b), which leads to an extra absorption peak between the upper branch (UB) and lower branch (LB) formed by surplus excitons. For simplification, the height is assumed as 35 nm. The influences caused by incidence angle and the substrate thickness on the quasi-BIC resonance are also performed. (See Figs. S1(a) and S1(b) in the Supplemental Material [37].)

To realize strong coupling, we consider not only the background refractive index but also the exciton refractive index in the following calculation. As displayed in Fig. 4(a), we perform a rich collection of hybrid-mode absorption spectra with the asymmetry parameters $\alpha = 0.17$ and $H = 35$ nm. There are two peaks marked with UB and LB in each absorption spectrum, showing evidence of strong coupling via changing the period of the nanodisk unit cell. Meanwhile, these peaks exhibit a slight redshift owing to the increase of the effective refractive index. It is worth noting that there is another smaller peak between these two peaks in the absorption spectrum, which represents the exciton not coupled to the MD quasi-BIC mode. These results can also be observed in the anticrossings of the two-dimensional color map, as depicted in Fig. 4(b).

Since the numerical simulations can be explained by the semi-analytical model [38–41], we construct a Hamiltonian model based on the temporal coupled-mode theory to describe

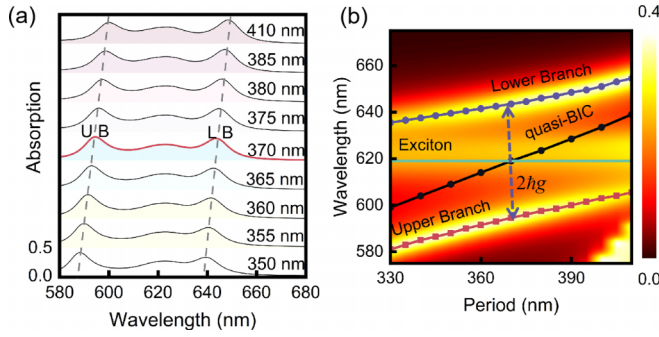


FIG. 4. (a) Absorption spectrum of the bulk WS₂ metasurface for different periods P at $\alpha = 0.17$ and $H = 35$ nm. (b) Simulated absorption contour map with different periods P at $\alpha = 0.17$ and $H = 35$ nm, where the green line and black line (dots) represent the individual exciton and magnetic dipole (MD) quasibound state in the continuum (BIC) mode; blue dashed dots (lines) and red dashed dots (lines) are the simulated (fitted) results of the upper branch (UB) and lower branch (LB), respectively.

the above simulation results [42]. This model consists of three modes: a MD quasi-BIC mode of the lossless cavity, a coupling-involved exciton, and a surplus exciton. Thus, this system response can be written as a complex amplitude $|a\rangle = (a_{\text{quasi-BIC}}, a_{\text{exciton}}, a_{\text{surplus}})^T$, and the dynamic equation can be given in the following step:

$$\frac{d|a\rangle}{dt} = \hat{H}|a\rangle + \hat{D}^T|s_+\rangle, \quad (2)$$

$$|s_-\rangle = \hat{C}|s_+\rangle + \hat{D}|a\rangle, \quad (3)$$

where $|s_+\rangle = [s_{1+}, s_{2+}]^T$ and $|s_-\rangle = [s_{1-}, s_{2-}]^T$ describe amplitudes of incoming and outgoing waves. Here, \hat{C} is the direct scattering matrix. The radiated coupling matrix $\hat{D} = \begin{pmatrix} \sqrt{\gamma_B} & 0 & 0 \\ \sqrt{\gamma_B} & 0 & 0 \end{pmatrix}$, and \hat{H} is the Hamiltonian of the coupled system:

$$\hat{H} = i \begin{pmatrix} \omega_B + i\gamma_B & g & 0 \\ g & \omega_E + i\gamma_E & 0 \\ 0 & 0 & \omega_{\text{surplus}} + i\gamma_{\text{surplus}} \end{pmatrix}, \quad (4)$$

where ω_B and γ_B are the frequency and half-widths of the quasi-BIC mode, respectively. Here, ω_E (ω_{surplus}) and γ_E (γ_{surplus}) represent the frequencies and half-widths of the excitons involved in coupling (surplus excitons), respectively. Also, g is the coupling strength. By calculating $\hat{H}|a\rangle = \omega|a\rangle$, the three energies of the UB, LB, and surplus exciton can be described as

$$\Omega_{\text{LB}} = \frac{1}{2}(i\gamma_B + i\gamma_E + \omega_B + \omega_E) - \sqrt{4g^2 + [\omega_B - \omega_E + i(\gamma_B + \gamma_E)]^2}, \quad (5)$$

$$\Omega_{\text{UB}} = \frac{1}{2}(i\gamma_B + i\gamma_E + \omega_B + \omega_E) + \sqrt{4g^2 + [\omega_B - \omega_E + i(\gamma_B + \gamma_E)]^2}, \quad (6)$$

$$\Omega_{\text{surplus}} = i\gamma_{\text{surplus}} + \omega_E. \quad (7)$$

With the condition $\hbar\omega_B = \hbar\omega_{\text{surplus}} = \hbar\omega_E = 2$ eV, these expressions can be further described as

$$\Omega_{\text{LB}} = \frac{1}{2}(i\gamma_B + i\gamma_E + 2\omega_E - \sqrt{4g^2 - \gamma_B^2 + 2\gamma_B\gamma_E - \gamma_E^2}), \quad (8)$$

$$\Omega_{\text{UB}} = \frac{1}{2}(i\gamma_B + i\gamma_E + 2\omega_E + \sqrt{4g^2 - \gamma_B^2 + 2\gamma_B\gamma_E - \gamma_E^2}), \quad (9)$$

$$\Omega_{\text{surplus}} = i\gamma_{\text{surplus}} + \omega_E. \quad (10)$$

The Rabi splitting can be given by

$$\hbar\Omega = \hbar\Omega_{\text{UB}} - \hbar\Omega_{\text{LB}} = \sqrt{4g^2 - (\gamma_B - \gamma_E)^2}. \quad (11)$$

Taking the red line in Fig. 4(a) as an example, the UB is ~ 595 nm, and the LB is ~ 644 nm, and the Rabi splitting $\hbar\Omega = \hbar\Omega_{\text{UB}} - \hbar\Omega_{\text{LB}} \approx 159$ meV, which is larger than the conventional Rabi splitting formed in monolayer TMDCs integrated on dielectric resonators [28,31]. The exciton mode involved in coupling can be defined as the difference between the total excitons γ_{total} and the surplus excitons γ_{surplus} . By calculating the half value of the full width at half maximum, we can obtain $\hbar\gamma_{\text{total}} = 38.1$ meV and $\hbar\gamma_{\text{surplus}} = 22.4$ meV; thus, $\hbar\gamma_E = \hbar\gamma_{\text{total}} - \hbar\gamma_{\text{surplus}} = 15.7$ meV. Because $\hbar\gamma_B = 14.3$ meV can be extracted by fitting the numerical simulation transmission spectrum T with the Fano model shown in Fig. 2 (e), we can obtain the coupling strength $\hbar g = 66.16$ meV by fitting the simulated results through Eqs. (5) and (6), which satisfies the condition of strong coupling $g > \frac{\gamma_B - \gamma_E}{2}$.

In addition, we can tune the interaction between excitons and quasi-BICs from weak to strong coupling by adjusting the asymmetry parameters in the following discussion. Considering an extreme example that γ_B as a linewidth is vanishingly small, which represents the coupling strength $\hbar g = 0$, the absorption will exhibit a pure exciton mode because the ideal BIC is a dark mode that does not couple with any exciton mode. This can also be achieved from Eqs. (8)–(10); when $\hbar\gamma_B = 0$ meV and $\hbar g = 0$ meV, these equations can be deduced: $\Omega_{\text{LB}} = \omega_E$, $\Omega_{\text{UB}} = i\gamma_E + \omega_E$, $\Omega_{\text{surplus}} = i\gamma_{\text{surplus}} + \omega_E$. This means the UB and LB degenerate into ideal BIC and exciton modes, respectively, resulting in a pure exciton mode without the splitting peaks in the absorption spectrum. When we set a smaller asymmetry parameter for the BIC, it will couple to the exciton mode, enabling the system to first enter the weak-coupling region. This can be captured by the blue area with $\alpha = 0.03$ in Fig. 5. It is worth noticing that the absorption of the UB and LB is close to zero, which means the number of photons is much less than excitons, leading to surplus excitons playing a dominant role in the absorption spectrum. As γ_B becomes larger, we can obtain three solutions from Eqs. (8) and (9), which means the system enters the strong-coupling region with the appearance of the spectral splitting. This can be proved by the other cases with $\alpha = 0.07, 0.17$, and 0.21 in Fig. 5. We can see that, with the increase of the asymmetry parameter, the absorption of the UB and LB increases synchronously, while the absorption of the surplus exciton mode decreases significantly. This is because the number of photons that can participate in the coupling become larger but are still less than the total excitons, resulting

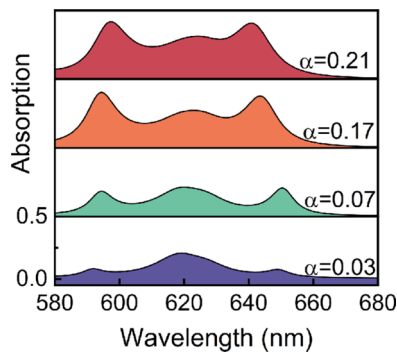


FIG. 5. Absorption spectra of the bulk WS_2 metasurface for different asymmetry parameters under the energy detuning of zero.

in a peak of the surplus exciton mode always existing in the absorption spectrum.

IV. CONCLUSIONS

In conclusion, we realize the strong coupling between MD quasi-BIC and excitons occurs within the proposed bulk WS_2 metasurface with the Rabi splitting up to 159 meV. Further, we describe the coupling scene by constructing a

Hamiltonian model containing the surplus excitons based on the temporal coupled mode theory, enabling a discussion of the coupling state evolution through considering surplus excitons. Our work could deepen understanding of the surplus exciton mode and the absorption manipulation in the strong light-matter interaction, which provides a theoretical contribution to designable exciton-polariton devices.

ACKNOWLEDGMENTS

This paper is supported by the National Natural Science Foundation of China (Grants No. 11947065, No. 12064025, and No. 12264028), the Natural Science Foundation of Jiangxi Province (Grants No. 20202BAB211007 and No. 20212ACB202006), the Key Research and Development Program of Jiangxi Province (Grant No. 20192BBE50058), the Interdisciplinary Innovation Fund of Nanchang University (Grant No. 20199166-27060003), the Open Project of Shandong Provincial Key Laboratory of Optics and Photonic Devices (Grant No. K202102), the Major Discipline Academic and Technical Leaders Training Program of Jiangxi Province (Grant No. 20204BCJ22012).

- [1] H. Deng, H. Haug, and Y. Yamamoto, *Rev. Mod. Phys.* **82**, 1489 (2010).
- [2] J. Kasprzak, M. Richard, S. Kundermann, A. Baas, P. Jeambrun, J. M. J. Keeling, F. M. Marchetti, M. H. Szymańska, R. André, J. L. Staehli *et al.*, *Nature* **443**, 409 (2006).
- [3] A. Amo, J. Lefrère, S. Pigeon, C. Adrados, C. Ciuti, I. Carusotto, R. Houdré, E. Giacobino, and A. Bramati, *Nat. Phys.* **5**, 805 (2009).
- [4] A. Amo, T. C. H. Liew, C. Adrados, R. Houdré, E. Giacobino, A. V. Kavokin, and A. Bramati, *Nat. Photon.* **4**, 361 (2010).
- [5] R. Su, C. Diederichs, J. Wang, T. C. H. Liew, J. Zhao, S. Liu, W. Xu, Z. Chen, and Q. Xiong, *Nano Lett.* **17**, 3982 (2017).
- [6] D. S. Dovzhenko, S. V. Ryabchuk, Y. P. Rakovich, and I. R. Nabiev, *Nanoscale* **10**, 3589 (2018).
- [7] S. Zu, B. Li, Y. Gong, Z. Li, P. M. Ajayan, and Z. Fang, *Adv. Opt. Mater.* **4**, 1463 (2016).
- [8] K. As'ham, I. Al-Ani, L. Huang, A. E. Miroshnichenko, and H. T. Hattori, *ACS Photonics* **8**, 489 (2021).
- [9] S. B. Anantharaman, K. Jo, and D. Jariwala, *ACS Nano* **15**, 12628 (2021).
- [10] Y. M. Qing, Y. Ren, D. Lei, H. F. Ma, and T. J. Cui, *J. Opt.* **24**, 024009 (2022).
- [11] L. Huang, A. Krasnok, A. Alú, Y. Yu, D. Neshev, and A. E. Miroshnichenko, *Rep. Prog. Phys.* **85**, 046401 (2022).
- [12] I. A. M. Al-Ani, K. As'ham, O. Klochan, H. T. Hattori, L. Huang, and A. E. Miroshnichenko, *J. Opt.* **24**, 053001 (2022).
- [13] P. Xie, Y. Wu, Y. Li, P. Chang, H. Zhang, and W. Wang, *J. Opt.* **24**, 093001 (2022).
- [14] J. T. Hugall, A. Singh, and N. F. van Hulst, *ACS Photonics* **5**, 43 (2018).
- [15] S. Xiao, T. Wang, T. Liu, C. Zhou, X. Jiang, and J. Zhang, *J. Phys. D: Appl. Phys.* **53**, 503002 (2020).
- [16] R. Sarma, J. Xu, D. de Ceglia, L. Carletti, S. Campione, J. Klem, M. B. Sinclair, M. A. Belkin, and I. Brener, *Nano Lett.* **22**, 896 (2022).
- [17] A. I. Kuznetsov, A. E. Miroshnichenko, M. L. Brongersma, Y. S. Kivshar, and B. Luk'yanchuk, *Science* **354**, aag2472 (2016).
- [18] Y. Chen, S. Miao, T. Wang, D. Zhong, A. Saxena, C. Chow, J. Whitehead, D. Gerace, X. Xu, S.-F. Shi *et al.*, *Nano Lett.* **20**, 5292 (2020).
- [19] K. Koshelev and Y. Kivshar, *ACS Photonics* **8**, 102 (2021).
- [20] F. Yesilkoy, E. R. Arvelo, Y. Jahani, M. Liu, A. Tittl, V. Cevher, Y. Kivshar, and H. Altug, *Nat. Photonics* **13**, 390 (2019).
- [21] A. Barreda, C. Zou, A. Sinelnik, E. Menshikov, I. Sinev, T. Pertsch, and I. Staude, *Opt. Mater. Express* **12**, 3132 (2022).
- [22] J. Kühne, J. Wang, T. Weber, L. Kühner, S. A. Maier, and A. Tittl, *Nanophotonics* **10**, 4305 (2021).
- [23] S. Xiao, M. Qin, J. Duan, F. Wu, and T. Liu, *Phys. Rev. B* **105**, 195440 (2022).
- [24] K. L. Koshelev, S. K. Sychev, Z. F. Sadrieva, A. A. Bogdanov, and I. V. Iorsh, *Phys. Rev. B* **98**, 161113(R) (2018).
- [25] K. Koshelev, S. Lepeshov, M. Liu, A. Bogdanov, and Y. Kivshar, *Phys. Rev. Lett.* **121**, 193903 (2018).
- [26] S. Cao, H. Dong, J. He, E. Forsberg, Y. Jin, and S. He, *J. Phys. Chem. Lett.* **11**, 4631 (2020).
- [27] I. A. M. Al-Ani, K. As'ham, L. Huang, A. E. Miroshnichenko, and H. T. Hattori, *Laser Photonics Rev.* **15**, 2100240 (2021).
- [28] M. Qin, S. Xiao, W. Liu, M. Ouyang, T. Yu, T. Wang, and Q. Liao, *Opt. Express* **29**, 18026 (2021).
- [29] P. Xie, Z. Liang, T. Jia, D. Li, Y. Chen, P. Chang, H. Zhang, and W. Wang, *Phys. Rev. B* **104**, 125446 (2021).
- [30] X. Zhang and A. L. Bradley, *Phys. Rev. B* **105**, 165424 (2022).

- [31] M. Qin, J. Duan, S. Xiao, W. Liu, T. Yu, T. Wang, and Q. Liao, *Phys. Rev. B* **105**, 195425 (2022).
- [32] R. Verre, D. G. Baranov, B. Munkhbat, J. Cuadra, M. Käll, and T. Shegai, *Nat. Nanotechnol.* **14**, 679 (2019).
- [33] J. Wang, W. Yang, G. Sun, Y. He, P. Ren, and Z. Yang, *Photonics Research* **10**, 1744 (2022).
- [34] B. Munkhbat, D. G. Baranov, M. Stührenberg, M. Wersäll, A. Bisht, and T. Shegai, *ACS Photonics* **6**, 139 (2019).
- [35] X. Zong, L. Li, and Y. Liu, *Opt. Lett.* **46**, 6095 (2021).
- [36] S. Wang, Q. Le-Van, F. Vaianella, B. Maes, S. E. Barker, R. H. Godiksen, A. G. Curto, and J. G. Rivas, *ACS Photonics* **6**, 286 (2019).
- [37] See Supplemental Material at <http://link.aps.org/supplemental/10.1103/PhysRevB.107.045417> for the influences of incidence angle and the substrate thickness on the quasi-BIC resonance.
- [38] C. A. Valagiannopoulos and P. Alitalo, *Phys. Rev. B* **85**, 115402 (2012).
- [39] O. Tsilipakos, T. Christopoulos, and E. E. Kriezis, *J. Lightwave Technol.* **34**, 1333 (2016).
- [40] N. L. Tsitsas and C. A. Valagiannopoulos, *J. Opt. Soc. Am. B* **34**, D1 (2017).
- [41] M. Hesari-Shermeh, B. Abbasi-Arand, and M. Yazdi, *Opt. Express* **29**, 1694 (2021).
- [42] S. Fan, W. Suh, and J. D. Joannopoulos, *J. Opt. Soc. Am. A* **20**, 569 (2003).